Available online at www.sciencedirect.com
ScienceDirect
International Journal of Mass Spectrometry 268 (2007) 304–315
International Journal of Mass Spectrometry
www.elsevier.com/locate/ijms

# Molecular characterization of myelin protein zero in *Xenopus laevis* peripheral nerve: Equilibrium between non-covalently associated dimer and monomer

Bo Xie [a,1], Xiaoyang Luo [b], Cheng Zhao [a,2], Christina Marie Priest [b,3], Shiu-Yung Chan [a], Peter B. O'Connor [a], Daniel A. Kirschner [b], Catherine E. Costello [a,*]

[a] *Mass Spectrometry Resource, Boston University School of Medicine, Boston, MA, United States*
[b] *Boston College, Chestnut Hill, MA, United States*

Received 19 March 2007; received in revised form 12 August 2007; accepted 15 August 2007
Available online 19 August 2007

**Abstract**

Myelin protein zero (P0), a glycosylated single-pass transmembrane protein, is essential in the formation and maintenance of peripheral nervous system (PNS) compact myelin. P0 in *Xenopus* (xP0) exists primarily as a dimeric form that remains stable after various physical and chemical treatments. In exploring the nature of the interactions underlying the dimer stability, we found that xP0 dimer dissociated into monomer during continuous elution gel electrophoresis and conventional SDS-PAGE, indicating that the dimer is stabilized by non-covalent interactions. Furthermore, as some of the gel-purified monomer re-associated into dimer on SDS-PAGE gels, there is likely a dynamic equilibrium between xP0 dimer and monomer *in vivo.* Because the carbohydrate and fatty acyl moieties may be crucial for the adhesion role of P0, we used sensitive mass spectrometry approaches to elucidate the detailed *N*-glycosylation and *S*-acylation profiles of xP0. Asn92 was determined to be the single, fully-occupied glycosylation site of xP0, and a total of 12 glycans was detected that exhibited new structural features compared with those observed from P0 in other species: (1) the neutral glycans were composed mainly of high mannose and hybrid types; (2) 5 of 12 were acidic glycans, among which three were sialylated and the other two were sulfated; (3) none of the glycans had core fucosylation; and (4) no glucuronic acid, hence no HNK-1 epitope, was detected. The drastically different carbohydrate structures observed here support the concept of the species-specific variation in *N*-glycosylation of P0. Cys152 was found to be acylated with stearoyl (C18:0), whereas palmitoyl (C16:0) is the corresponding predominant fatty acyl group on P0 from higher vertebrates. We propose that the unique glycosylation and acylation patterns of *Xenopus* P0 may underlie its unusual dimerization behavior. Our results should shed light on the understanding of the phylogenetic development of P0's adhesion role in PNS compact myelin.


*Keywords:* De novo *N*-linked glycan sequencing; Mass spectrometry; Species-specific *N*-glycosylation

*Abbreviations:* CAD, collision-activated dissociation; α-CHCA, α-cyano-4-hydroxycinnamic acid; CHAPSO, 3-[(3-cholamidopropyl) dimethylammonio]-2-hydroxy-1-propane sulfonate; CHN, congenital hypomyelination neuropathy; CID, collision-induced decomposition; CMT1B, Charcot Marie Tooth disease 1B; DHB, 2,5-dihydroxybenzoic acid; DSS, Dejerine-Sottas syndrome; DTMAB, dodecyltrimethylammonium bromide; ED, extracellular domains; ESI-QoTOF MS, electrospray ionization quadrupole-orthogonal time-of-flight mass spectrometer; ER, endoplasmic reticulum; FTMS, Fourier transform mass spectrometry; HNK, human natural killer; ICR, ion cyclotron resonance; MAG, myelin-association glycoprotein; MALDI-TOF MS, matrix-assisted laser desorption/ionization TOF mass spectrometry; MPZ, myelin protein zero gene; beta-OG, *n*-octylbetaglucoside; PGC, porous graphite column; PNGase F, peptide *N*-glycosidase F; PNS, peripheral nervous system; P0, Protein zero; PTMs, post-translational-modifications; SDS-PAGE, Sodium dodecyl sulfate-polyacrylamide gel electrophoresis; TFA, trifluoroacetic acid; xP0, *Xenopus laevis* myelin protein zero

* Corresponding author at: Center for Biological Mass Spectrometry, Departments of Biochemistry and Biophysics, Boston University School of Medicine, 670 Albany St, Rm. 511, Boston, MA 02118, United States. Tel.: +1 617 638 6490; fax: +1 617 638 6491.
*E-mail address:* cecmsms@bu.edu (C.E. Costello).
[1] Present address: Achaogen, Inc., South San Francisco, CA 94080, United States.
[2] Present address: Abbott Laboratories, Abbott Park, IL 60064, United States.
[3] Present address: Department of Biological Sciences, Columbia University, New York, NY 10027, United States.

1387-3806/$ – see front matter © 2007 Elsevier B.V. All rights reserved.
doi:10.1016/j.ijms.2007.08.007

## 1. Introduction

Myelin protein zero (P0) is the most abundant protein in the peripheral nerve myelin of vertebrates. It plays an essential role in the formation and maintenance of peripheral nervous system (PNS) compact myelin. Mutations in the myelin protein zero gene (MPZ) can lead to a broad spectrum of inherited peripheral neuropathies such as Charcot Marie Tooth disease 1B (CMT1B), Dejerine-Sottas syndrome (DSS), and congenital hypomyelination neuropathy (CHN) (Inherited Peripheral Neuropathies Mutation Database, http://molgen-ww.uia.ac.be/CMTMutations/), either by interfering with normal P0 homophilic interactions or by producing abnormal myelin sheath [1–4].

P0 is an integral membrane glycoprotein, containing an extracellular domain that harbors a single *N*-glycosylation site, a single-pass transmembrane domain, and a cytoplasmic tail with a single acylation site located near the junction of the presumed transmembrane and cytoplasmic domains. A number of *in vitro* studies of transfected cultured cells have shown that *N*-linked carbohydrate moieties are crucial for the adhesion role of P0 through homophilic interactions [5–7]. For example, when compared with other non-glycosylated peptides, only the peptide fragment containing an unoccupied glycosylation site resulted in significant inhibition of cell adhesion [8]. Furthermore, non-glycosylated P0 produced by site-directed mutagenesis at the glycosylation site does not show homophilic adhesion [7]. In addition to glycosylation, the covalently bound long-chain fatty acyl group on Cys153 also appears to be very important for normal P0 homophilic interactions; it has been proposed that acylation promotes association of P0 with the underlying cytoskeleton in a manner similar to that shown for other glycoproteins [9–12].

Crystallographic and small angle X-ray scattering suggest that P0 exists primarily as tetramers in the peripheral myelin of higher vertebrates such as murine and bovine [13,14]. However, in sciatic nerve myelin of *Xenopus laevis*, the classic amphibian model organism, dimeric P0 is the predominant and most stable form [15–17]. The level of *Xenopus* P0 (xP0) dimer is apparently unaffected by a variety of physical (temperature) and chemical (pH, detergents, denaturants, and reduction/alkylation) treatments, suggesting that the underlying force stabilizing the dimer may be a non-disulfide covalent bond [15].

To test this hypothesis, we undertook a detailed MS analysis of xP0 dimer and monomer. When the peptide mass fingerprints obtained following in-gel proteolysis of dimer and monomer were compared with one another, no cross-linked peptides were identified, although more than 60% amino acid sequence coverage was achieved. Continuous elution gel electrophoresis was then performed to achieve large-scale purification of sufficient xP0 dimer to enable solution proteolysic digestion that could extend the sequence coverage through further MS analyses. However, we found that nearly all the dimer dissociated into monomer during the prolonged elution process. Furthermore, both dimer and monomer were found to be present in significant amounts on the slab gel when either gel-extracted dimer or monomer was analyzed. This result suggested both that the xP0 dimer is stabilized by non-covalent interaction(s) and that an equilibrium between the dimer and the monomer may exist in the native myelin.

To further explore the molecular basis of P0 dimer formation in *Xenopus*, we investigated two important protein post-translational-modifications (PTMs), glycosylation and acylation, which are typically involved in protein interaction and oligomerization. The detailed glycosylation profile of xP0 was elucidated using a sensitive approach that combined in-gel glycosidase and protease digestions, permethylation of released glycans, and mass spectrometry. Here, we report, for the first time, the native glycoforms of xP0. The major glycan structures were characterized with high mass accuracy by ESI-FT MS/MS (CAD). Asn92 (corresponding to Asn93 in higher vertebrates, Supplementary Fig. 2) was identified as the single, fully-occupied *N*-glycosylation site by ESI-MS/MS. It was found to bear a series of non-fucosylated neutral, silalylated glycans and minor amounts of sulfated oligosaccharides. This glycan profile was remarkably different from those observed in P0 from human and bovine sources, in which sulfated *N*-acetylglucosamine is present at a significant level, and all glycans show core-fucosylation. We postulate that the divergence in glycoform distributions among different species may imply an evolutionary change in the *N*-glycosylation pattern of P0. In addition, we determined that Cys152 (Cys153 in higher vertebrates, Supplementary Fig. 2) was acylated predominantly with stearoyl, whereas in the higher vertebrates (murine and bovine), palmitoyl is the major fatty acyl modificaton [10,11]. We propose that the unique glycosylation and acylation profiles of P0 in *Xenopus* may be responsible for its unusual dimerization behavior in PNS myelin. These results should contribute to understanding the phylogenetic development of P0's adhesion role in PNS compact myelin.

## 2. Experimental

### 2.1. Materials

Chemicals and their sources are listed below. Enzymes including recombinant, glycerol-free endoglycosidase PNGase F (New England Biolabs Inc., Beverly, MA), sequencing grade endoproteinases trypsin (Princeton Separations, Adelphia, NJ), Asp-N, and Lys-C and Glu-C (Roche Molecular Biochemicals, Indianapolis, IN) were used for in-gel digestions. The matrices used for matrix-assisted laser desorption/ionization reflectron time-of-flight mass spectrometry (MALDI-TOF MS) analyses were 2,5-dihydroxybenzoic acid (2,5-DHB), α-cyano-4-hydroxycinnamic acid (α-CHCA) (Bruker, Billerica, MA), and D-arabinosazone prepared from phenyl hydrazine and D-arabinose (Sigma–Aldrich, St. Louis, MO). The permethylation reagents dimethyl sulfoxide, sodium hydroxide, and methyl iodide, as well as chloroform and other solvents (Sigma–Aldrich), were stored under dry conditions.

### 2.2. Methods

#### 2.2.1. Myelin isolation from Xenopus laevis peripheral nerve

Sciatic nerves were dissected from adult female *Xenopus laevis* (NASCO, Fort Atkinson, WI) and homogenized with a Dounce homogenizer in aprotinin/water to prevent proteolysis. Myelin was isolated and purified using a discontinuous 0.32 M/0.85 M sucrose density gradient, reconstituted in 0.5 μg/ml aprotinin/water, and stored at −80 °C prior to use [18,19].

#### 2.2.2. SDS-PAGE

Samples were dissolved in SDS sample buffer (0.5 M Tris–HCl, pH 8.6, 0.1% bromophenol blue, glycerol, water) (Invitrogen, Carlsbad, CA); the solution was boiled for 5 min, and cooled to room temperature before being loaded on 10 or 4–20% pre-cast Tris–HCl polyacrylamide gels (Invitrogen, Carlsbad, CA) using an E 19001-Xcell II Mini-Cell (Genisphere Inc., Hatfield, PA). All gels were run at 125 V constant voltage and were stained with GelCode Blue Stain reagent (Pierce, Rockford, IL), followed by destaining with deionized water.

#### 2.2.3. Protein in-gel extraction

Protein bands of interest were excised from the gel and minced into fine pieces. Proteins were extracted from the gel pieces using a buffer containing 100 mM Tris–HCl, pH 8.5, 0.1% SDS for 12 h at room temperature with constant shaking, followed by another 12-h incubation in newly exchanged buffer. Extraction solutions were then completely removed in an SC 110 SpeedVac™ concentrator (Savant Instruments, Farmingdale, NY) and re-dissolved in SDS sample buffer before being reloaded onto SDS-PAGE gels.

#### 2.2.4. P0 purification using Mini-Prep-Cell™

P0 protein was purified from isolated *Xenopus* sciatic nerve myelin using a Mini Prep Cell™ (Bio-Rad, Hercules, CA) containing a 10% polyacrylamide column gel (5 cm separating gel; 1.5 cm, 4% stacking gel; 1 cm diameter) equipped with a peristaltic pump and a fraction collector. Myelin sample was first subjected to electrophoresis on the column gel at 200 V constant voltage. Approximately 80 eluted protein fractions, 1.5 ml each, were then collected by the fraction collector with a 100 μl/min flow rate and analyzed for protein content by SDS-PAGE.

#### 2.2.5. Protein in-gel reduction and alkylation

The excised gel bands were cut into pieces of about 1 $mm^3$ and washed with 50 mM $NH_4HCO_3$ followed by 100% acetonitrile. After removal of the supernatant, gel pieces were completely dried in a SpeedVac™ and then incubated at 56 °C for 60 min in 25 μl of 10 mM dithiothreitol (in 50 mM $NH_4HCO_3$) for protein reduction. After cooling of the digestion mixture to room temperature and removal of the supernatant, the gel pieces were incubated at 45 °C for 45 min in the dark with 25 μl of 50 mM fresh iodoacetamide (in 50 mM $NH_4HCO_3$) for alkylation of the free Cys residues. Gel pieces were then washed in 50 μl of 50 mM $NH_4HCO_3$, followed by 100% $CH_3CN$ to remove SDS, reducing and alkylation reagents, and dried in a SpeedVac™.

#### 2.2.6. In situ glycosidase and protease digestions

The dried gel pieces were treated with PNGase F (500 units/ml in 25 mM $NH_4HCO_3$), followed by a protease, including trypsin, Asp-N, Endo Lys-C, and Endo Glu-C. For each digestion, the volume of enzyme solution was adjusted to cover the gel pieces, then more incubation buffer (50 mM $NH_4HCO_3$) was added, and the tubes were incubated at 37 °C overnight.

#### 2.2.7. Oligosaccharide and peptide extractions

Glycans were extracted from the gel pieces by removing the incubation buffer, which already may have contained some sugars, and using three exchanges of 100 μl water, with sonication for 30 min each time. All supernatants were combined and dried in a SpeedVac. Peptides were extracted from the gel pieces following a similar procedure, except that 100 μl 50% acetonitrile was used instead of water.

#### 2.2.8. Purification of glycans

The released glycans were further purified by a porous graphite column (PGC) (Harvard Apparatus, Holliston, MA). The column was washed prior to the loading of the fresh water-reconstituted glycan samples [20]. Glycans were then recovered from the column with three changes of 100 μl of acetonitrile:water:trifluoroacetic acid (TFA) (25:75:0.05, v:v:v) followed by three changes of 100 μl of acetonitrile:water:TFA (40:60:0.05, v:v:v) [21]. All fractions were combined and freeze-dried, then reconstituted in water prior to mass spectrometry analysis.

#### 2.2.9. Permethylation of glycans

Released glycans were dissolved in $Me_2SO$ and per-*O*-methylated by treating the sample with powdered sodium hydroxide plus methyl iodide using the method introduced by Ciucanu and Kerek [22] and modified by Ciucanu and Costello [23].

#### 2.2.10. Mass spectrometry

Mass spectra were acquired on a Bruker Reflex IV MALDI-TOF MS equipped with a Laser Science nitrogen laser (Bruker Daltonics, Billerica, MA) having a 3-ns pulse width at 337 nm, or an electrospray ionization (ESI) QSTAR Pulsar *i* quadrupole-orthogonal TOF mass spectrometer (MS and MS/MS) (Applied Biosystems, Foster City, CA), or a custom built ESI-qQq-FTMS [24,25].

*2.2.10.1. MALDI-TOF MS.* Dried native and permethylated glycans were dissolved in water and $CH_3CN$:water (70:30, v:v), respectively. One microliter of sample was then mixed with 1 μl of the MALDI matrix 2,5-DHB (10 mg/ml in $CH_3CN$:water:TFA (50:50:0.1, v:v:v)), spotted onto the MALDI target plate, allowed to dry and analyzed in the positive and negative reflectron modes with delayed extraction. Native and permethylated oligosaccharides were observed as $[M+Na]^+$

or $[M-H]^-$ ions. The spectra of native glycans with D-arabinosazone as matrix were acquired according to a similar procedure, except the matrix bulk solution was prepared by dissolving 1 mg D-arabinosazone in 50–200 ml ethanol or methanol. Zip-Tip$^{TM}$-cleaned protease digested peptides were dissolved in $CH_3CN$:water:TFA (50:50:0.1, v:v:v). One microliter of sample solution was mixed with the MALDI matrix α-CHCA (10 mg/ml in $CH_3CN$:water:TFA (50:50:0.1, v:v:v) or 2,5-DHB (10 mg/ml in $CH_3CN$:water:TFA (50:50:0.1, v:v:v), deposited on a MALDI target, and observed as $[M+H]^+$ in the positive ion spectra. External mass calibration was performed using a standard peptide mixture (Bruker, Billerica, MA) with known molecular masses.

*2.2.10.2. ESI-QoTOF-MS and MS/MS.* Nanospray needles were pulled from thin-wall borosilicate glass capillaries (1.2-mm orifice diameter; World Precision Instruments, Sarasota, FL) using a micropipette puller (Model P-97, Sutter Instruments Co., Novato, CA). Typically, peptides cleaned by passage through a Zip-Tip$^{TM}$ were eluted with $CH_3CN$:water:formic acid (50:50:0.5, v:v:v) and analyzed in the positive ion mode. Peaks whose measured masses suggested the presence of potential glycosylation sites were selected for MS/MS analyses. The instrument was calibrated using the monoisotopic $[M+2H]^{2+}$ *m/z* 785.843 of Glu-fibrinopeptide B, and the calibration for MS/MS experiments was performed using two monoisotopic fragment ions generated from the same $[M+2H]^{2+}$ of Glu-fibrinopeptide B.

*2.2.10.3. ESI Fourier transform (FT) MS/MS (CAD).* For structural analysis on released and permethylated glycans, a custom built qQq-FTMS with a nanospray source and 7T actively shielded magnet (Cryomagnetics Inc., Oak Ridge, TN) was utilized. The dried permethylated glycans were dissolved in 25 mM NaOH, 50% methanol (40:60, v:v). The sample (∼2 to 3 μl) was loaded into a glass capillary tip pulled with the micropipette puller to ∼1-μm orifice diameter and a stainless steel wire was inserted into the distal end of the tip to form the electrical connection. For Collision-Activated Dissociation (CAD) experiments, the parent ions were isolated by Q1, and were fragmented by collisions at relatively high energy (60–75 eV) with $N_2$ gas in Q2. The total pulse duration for CAD experiments varied between 1 and 2 s. All data were analyzed without apodization and with two zero-fills to improve mass accuracy. The MS/MS spectra were internally calibrated based on the $[M+2H]^{2+}$, $[M+H]^+$ ions and their isotopes. The ICR conditions used in this study were the same as those in prior publications [24,25].

## 3. Results

### 3.1. xP0 monomers were non-covalently associated into dimer

The dramatic stability of xP0 dimer shown in the previous study [15] led to our initial hypothesis that xP0 monomer is covalently associated to form dimer. Evidence supporting this proposition would be the discovery of a novel cross-linked peptide using mass spectrometry to analyze the products from proteolytic digestion of the dimer. To undertake this, xP0 dimer was first separated by 1D SDS-PAGE. Bands of interest were in-gel digested with multiple proteases, including trypsin, Asp-N, Lys-C, and Glu-C, each having different cleavage specificity, to achieve more sequence coverage and improve the likelihood for detecting the cross-linked peptide. Digestion was followed by MS analysis of the resulting peptide fragments. By comparing the fragments released from monomeric xP0 after the same enzymatic treatments with the dimer fragments, any peptide fragments containing the cross-linking site in the dimer would become apparent and then could be identified. However, we did not observe any difference between the MALDI-TOF MS profiles of the proteolytic peptides from dimer and monomer (trypsin, Asp-N digestions shown in Supplementary Fig. 1; Lys-C, Glu-C digestion data not shown). Thus, although more than 60% amino acid sequence coverage was obtained, no specific cross-linked peptide fragment was detected (Supplementary Fig. 2).

A potential problem of the in-gel digestion is that the larger peptide fragments, which might carry the cross-linking sites in xP0 dimer, would remain in the gel matrix after the extraction procedures. To circumvent this potential difficulty, an alternative strategy was adopted: continuous elution preparative gel electrophoresis using the Mini-Prep-Cell$^{TM}$ was used to purify P0 protein isolated from myelin on a large scale, and then the eluted dimer and monomer fractions would be subjected to protease digestions in solution. However, when the eluted fractions were analyzed by SDS-PAGE to profile their protein contents, nearly all xP0 dimer dissociated into monomer (Supplementary Fig. 3). These findings argued against the notion that the intermolecular cross-linking stabilized the dimer, and, moreover, suggested that *Xenopus* P0 monomer likely associates into dimer through very strong non-covalent interactions. This explanation was further supported by reloading gel-extracted dimer onto 4–20 or 10% slab gels, and finding that around half of the protein then appeared as monomer. Interestingly, when the converse experiment was performed on monomer extracted from the gel, a significant amount of xP0 dimer appeared (Fig. 1). These results not only substantiated the non-covalent nature of xP0 dimerization, but also suggested an apparent dynamic equilibrium between dimer and monomer on SDS-PAGE gels.

### 3.2. xP0 harbors a series of non-fucosylated neutral and sialylated glycans on Asn 92

To further understand the molecular mechanism of the dimerization process, we investigated the *N*-glycosylation profile of xP0. Glycans of xP0 dimer and monomer were released from the gel by PNGase F and then applied to the pre-washed PGC cartridge. The masses of the glycans, as revealed in the positive and negative ion MALDI mass spectra of native *N*-glycans from dimer that were obtained using DHB as the matrix (Fig. 2A and B, Table 1), corresponded to a series of neutral (I, II, III, IV, VI, VII and X, possibly high-mannose or hybrid glycans),sialylated

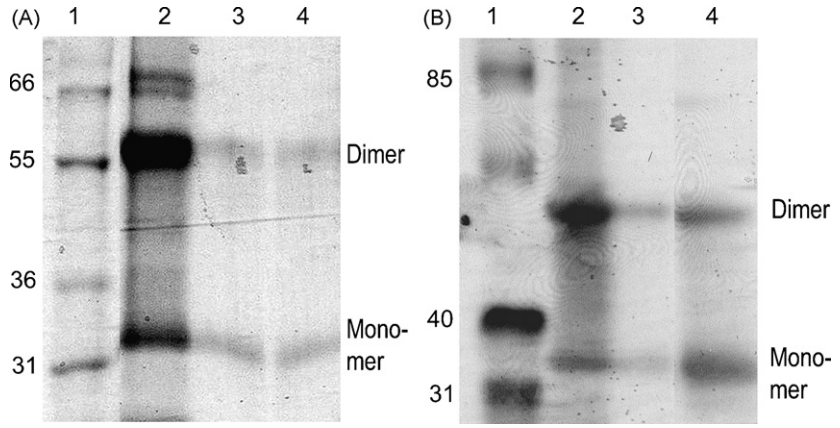


Fig. 1. SDS-PAGE analysis of gel purified xP0 dimer and monomer on (A) 10% and (B) 4–20% slab gels. Lane 1, markers with the numbers on the *left* denoting molecular weight in kDa; lane 2, purified sciatic nerve myelin from *Xenopus*; lane 3, gel-extracted xP0 monomer; lane 4, gel-extracted xP0 dimer.

(IX, XI and XII, possibly hybrid type), and sulfated glycans (V and VIII) based on comparison of their observed molecular weights and known *N*-linked glycans.

The glycans released from xP0 monomer (Fig. 2C) were similar to those from the dimer except that the sulfated glycans (V and VIII) were not observed, probably due to the low abundance of glycans recovered from in-gel digestion and further cleanup from the relatively faint monomer band in the gel.

Earlier reports on the use of various matrices have shown that use of D-arabinosazone as matrix produces good negative-ion MALDI spectra of acidic (e.g., sialylated and sulfated) glycans. Therefore, we studied the native glycans recovered from xP0 dimer and monomer, using D-arabinosazone that was prepared from phenylhydrazine and D-arabinose according to published procedures [21,26,27]. The profiles of neutral and acidic glycans in these spectra (Supplementary Fig. 4)

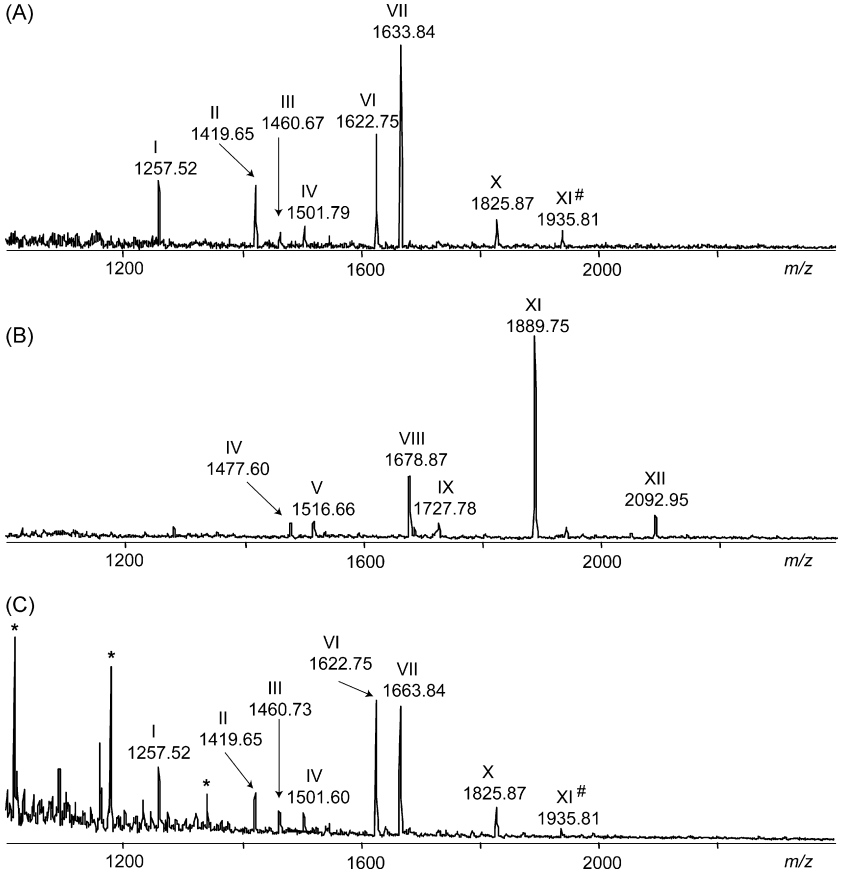


Fig. 2. Analysis of the *N*-linked native glycans of xP0 by MALDI-TOF MS (with 2,5-DHB matrix) in (A) positive mode and (B) negative mode from dimer, and (C) positive mode from monomer. Monoisotopic peaks are annotated. The numbers above the peaks are the monoisotopic masses and structure numbers are given in Table 1. In (A) and (C), all peaks correspond to $[M+Na]^+$, except when the # symbol indicates $[M-H+2Na]^+$; in (B), all peaks correspond to $[M-H]^-$. * indicates polyhexose contaminants.

Table 1
Proposed compositions and possible structures of the native and permethylated glycans released by in-gel PNGase F digestion of xP0 dimer and monomer, respectively

N-linked glycans from P0

| Number | Native glycans | | | | | Permethylated glycans | | | Composition | Proposed structure |
|---|---|---|---|---|---|---|---|---|---|---|
| | | | Dimer | | Monomer | | Dimer | Monomer | | |
| | $[M+Na]^+$ Calc. | $[M–H]^-$ calc. | $[M+Na]^+$ obs. | $[M–H]^-$ obs. | $[M+Na]^+$ obs. | $[M+Na]^+$ Calc. | $[M+Na]^+$ obs. | $[M+Na]^+$ obs. | | |
| 1 | 1257.52 | 1233.52 | 1257.52 | N.A | 1257.52 | 1579.78 | 1579.84 | 1579.84 | H5N2 | |
| II | 1419.57 | 1395.57 | 1419.65 | N.A | 1419.65 | 1783.88 | 1783.92 | 1783.82 | H6N2 | |
| III | 1460.60 | 1437.61 | 1460.67 | N.A | 1460.73 | 1824.91 | 1824.96 | 1824.96 | H5N3 | |
| IV | 1501.62 | 1477.63 | 1501.79 | 1477.60 | 1501.60 | 1865.94 | 1865.82 | 1865.85 | H4N4 | |
| V | N.A | 1516.56 | N.A | 1516.66 | N.A | N.A | N.A | N.A | H5N3S1 | |
| VI | 1622.65 | 1598.65 | 1622.75 | N.A | 1622.75 | 2029.01 | 2028.76 | 2028.76 | H6N3 | |
| VII[a] | 1663.68 | 1639.68 | 1663.84 | N.A | 1663.84 | 2070.04 | 2070.17 | 2070.17 | H5N4 | |
| VIM | N.A | 1678.61 | N.A | 1678.87 | N.A | N.A | N.A | N.A | H6N3S1 | |
| IX[a] | 1751.69 | 1727.70 | N.A | 1727.78 | N.A | 2186.08 | 2186.08 | 2186.08 | H5N3SA1 | |
| X | 1825.73 | 1801.73 | 1825.87 | N.A | 1825.87 | 2274.14 | 2274.09 | 2274.09 | H6N4 | |
| XI | 1935.72[b] | 1889.75 | 1935.81[b] | 1889.75 | 1935.81[b] | 2390.18 | 2390.25 | 2390.25 | H6N3SA1 | |
| XII | 2116.83 | 2092.83 | N.A | 2092.95 | N.A | 2635.31 | 2635.35 | 2635.40 | H6N4SA1 | |

Compositions and structures were tentatively assigned to MALDI-TOF MS peaks on the basis of *m/z* values, the normal *N*-linked glycan structures, and the structures of the major glycans were confirmed by ESI-FT MS/MS. Obs., observed monoisotopic mass; Calc., calculated monoisotopic mass. H, hexoses; N, HexNAc; SA, sialic acid (NeuAc); S, sulfate group.

[a] Glycans whose structures were confirmed by ESI-FT MS/MS (CAD).

[b] $[M-H+2Na]^+$ ion. N.A., not available.

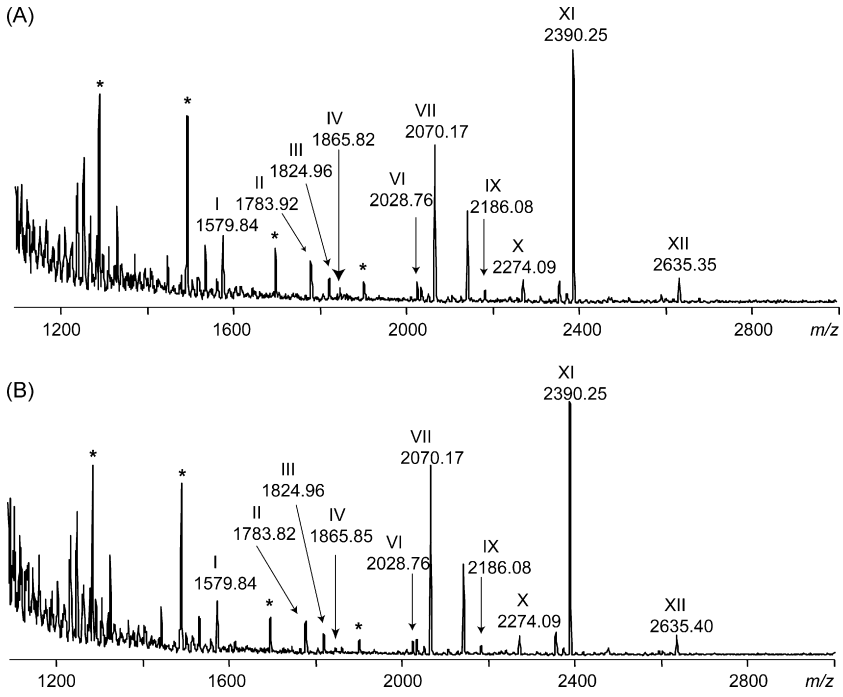


Fig. 3. Positive mode MALDI-TOF MS analysis of the permethylated glycans released from (A) P0 dimer and (B) monomer (2,5-DHB as matrix). Monoisotopic peaks are annotated. Numbers above the peaks are monoisotopic masses. The permethylated glycans (I–XII except V and VIII) here are consistent with the corresponding ones in Fig. 2 and summarized in Table 1. *, polyhexose contaminants.

were consistent with those acquired using 2,5-DHB as the matrix.

To increase the sensitivity of MS detection of the released glycans for detailed structural analyses in further MS/MS experiments, we subjected the glycans to permethylation. After permethylation, the profiles of the glycans from xP0 dimer and monomer (Fig. 3) were consistent with those of the native glycans except for the two sulfated species (V and VIII), because the sulfate groups were resistant to permethylation [28,29]. The calculated masses, proposed compositions, and the possible

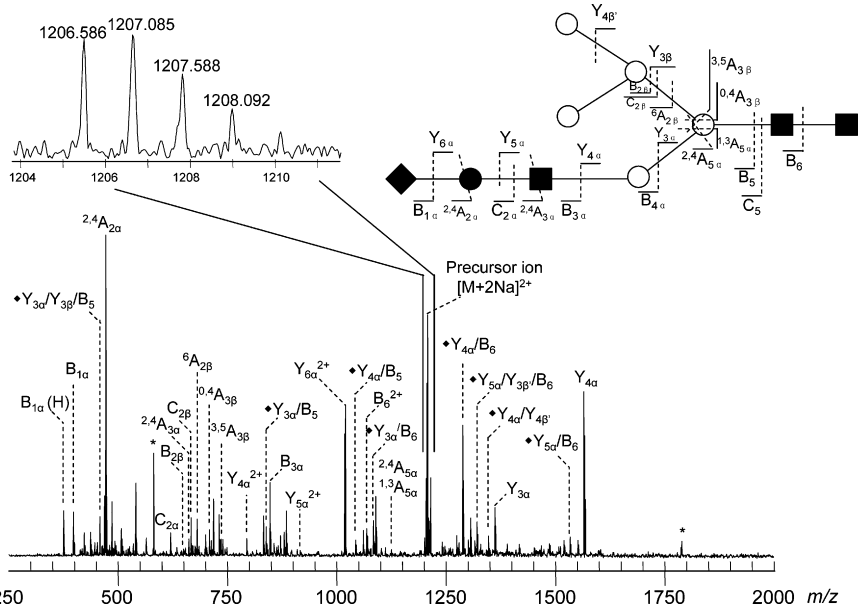


Fig. 4. Characterization of a permethylated glycan ion at *m/z* 1206.586, corresponding to glycan XI, by ESI-FT MS/MS (CAD). The illustrated glycan structure was assigned on the basis of the MS/MS fragmentation pattern, taking into account the usual *N*-linked glycan structures. Monoisotopic peaks are annotated. All fragments contain sodium except the one designated $B_{1\alpha}$(H). ♦, on the left of the assignment in the spectrum indicates that only one of the possible internal fragments is shown here. For each, the observed *m/z*, calculated *m/z*, error (ppm) between calculated and observed *m/z*, and corresponding assignment are listed in Supplementary Table 1. $^{6}A_{2\beta}$ indicates a cleavage between the carbon atoms 5 and 6 of the six-substituted mannose with charge retention on the non-reducing end; it is a complementary ion to W fragments [60]. Key to the symbols for the glycan structure in the upper panel: ■, *N*-acetylglucosamine (GlcNAc); ◯, mannose (Man); ●, galactose (Gal); ♦, *N*-acetylneuraminic acid (NeuAc).

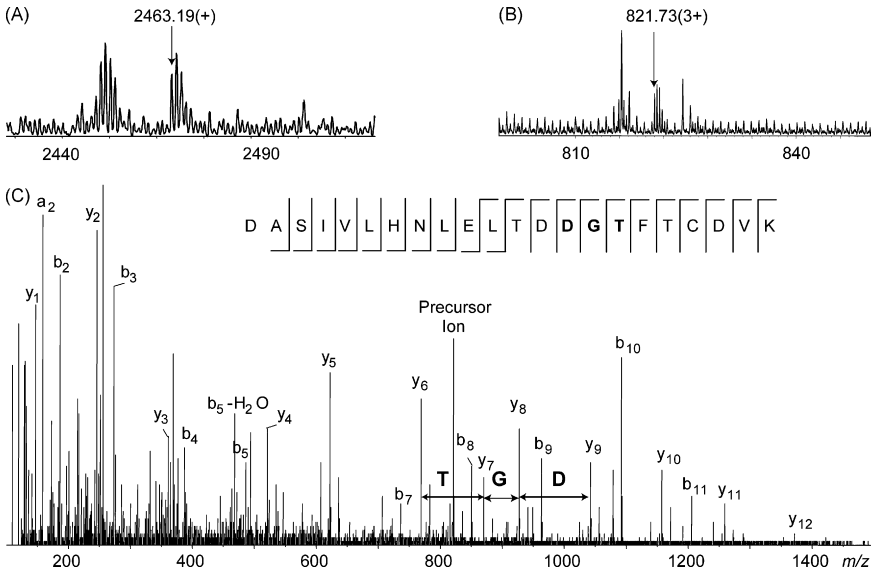


Fig. 5. Identification of Asn92 as a fully occupied *N*-glycosylation site of xP0 by MALDI-TOF MS and ESI-TOF MS analysis of the trypsin digested dimer (A) and monomer (B) after deglycosylation, and the detailed confirmation of the *N*-glycosylation motif by ESI-MS/MS (C). The peaks at *m/z* 2463.19(+) (A) and *m/z* 821.73(3+) (B) correspond to initially glycosylated peptides that undergo glycan loss and Asn (N) to Asp (D) conversion in the *N*-glycosylation motif (bold) upon deglycosylation by PNGase F, as shown in the scheme in (C). In (C), monoisotopic peaks are annotated, and the illustrated peptide sequence was derived from b- and y-ions in the MS/MS fragmentation pattern.

structures of various glycoforms from dimer and monomer are compiled in Table 1.

Furthermore, Fourier transform tandem mass spectrometry (FT-MS/MS) was used to study the structures of the permethylated glycans from xP0. The major glycans gave comprehensive fragmentation spectra. The highly accurate mass determinations obtained from ESI FT-MS/MS (CAD) allows unambiguous assignment of the fragmentation ions. Fig. 4 presents a representative positive-ion FT ESI MS/MS (CAD) spectrum of a glycan to which we assigned a sialylated hybrid structure (XI). Designations of fragments are based on the nomenclature for oligosaccharide fragmentation introduced by Domon and Costello (Supplementary Fig. 5) [30]. The glycan structure shown was deduced from its observed mass, the established common structures for the inner residues of *N*-linked glycans, and the glycosidic and cross-ring fragmentation patterns from MS/MS. The observed prominent glycosidic fragments such as B-, C-, Y-ions and cross-ring fragments such as $^{0,4}A_{3\beta}$ (*m/z* 709.325), $^{3,5}A_{3\beta}$ (*m/z* 737.358) strongly indicate that this is an asymmetric hybrid glycan with a sialic acid residue at one of the non-reducing termini (Supplementary Table 1). Further evidence for this assignment is the presence of internal fragments which provide detailed structural information on the major glycan fragments.

MALDI-TOF MS and ESI-QoTOF MS analyses mapped the *N*-glycosylation to Asn92 in the xP0 dimer and monomer by identifying a tryptic peptide that had undergone the expected Asn(N)92 to Asp(D)92 conversion upon deglycosylation, and the sequence of this peptide was confirmed by ESI-MS/MS. The peaks at *m/z* 2463.19(+) (Fig. 5A) and *m/z* 821.73(3+) (Fig. 5B) corresponded to deglycosylated peptides (residues 79–100) that had undergone glycan loss from the single *N*-glycosylation motif (Fig. 5C, bolded sequence in the upper diagram). The simple isotopic patterns observed for the peptide containing the consensus sequence indicated that it is fully glysosylated. The amino acid sequence of the deglycosylated peptide was confirmed by ESI-MS/MS (Fig. 5C, Supplementary Fig. 2).

### 3.3. Cys152 of xP0 was acylated by stearic acid

Cys152 was identified by MALDI-TOF MS as a fully occupied acylation site, modified predominantly by the stearoyl

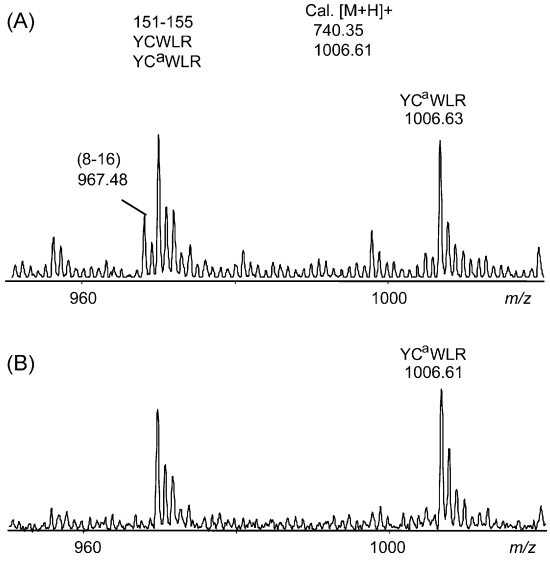


Fig. 6. Identification of acylation profile and acylation site in xP0 by MALDI-TOF MS. The peaks at *m/z* 1006.63 in dimer (A), and *m/z* 1006.61 in monomer (B) correspond to stearoylated (Δ266.26 u) tryptic peptides 151–155, as shown in the upper panel.

group (C18:0) in both dimer and monomer. The masses at *m*/*z* 1006.63 in the spectrum of the dimer (Fig. 6A), and 1006.61 in that of the monomer (Fig. 6B) are consistent with the tryptic peptide 151–155 after stearoylation (Δ266.26). Within this peptide (YCWLR), only Cys is a potential site of acylation. Therefore, our result suggests that Cys152, which is located at the junction between transmembrane and cytoplasmic domains of xP0, has a stearoyl modification. No evidence for acylation at other sites was found.

## 4. Discussion

P0 plays a central role in the formation and stability of both extracellular and cytoplasmic appositions of the compact PNS myelin. In the crystal, the extracellular domains of rat P0 (P0-ED) associate in a *cis* arrangement (in the plane of membrane) to form homotetramers and these tetramers interact with each other in a *trans* orientation (normal to the plane of the membrane) to form a highly ordered network [13]. Full length bovine P0 also assembles tetramerically in a membrane bilayer-mimetic, indicating that P0 protein from higher vertebrates likely exists as tetramers in the myelin membrane [14]. However, previous experiments using native PAGE to analyze *Xenopus* P0 identified a stable dimeric form [15]. This atypical oligomerization behavior aroused our initial curiosity about the molecular mechanism of P0 assembly in the compact PNS myelin of *Xenopus*.

### 4.1. Multiple non-covalent interactions could account for stability of xP0 dimer

Molecular modeling and the crystal structure of rat P0-ED suggest that His52 and Arg45′, which are conserved in *Xenopus* and higher vertebrate P0, are located at the putative dimeric interface of P0 *trans*-interaction and are thought to be critical for P0 homophilic interactions [13,31]. X-ray diffraction analysis of myelin structure and inter-membrane interaction as a function of pH and ionic strength showed that the native width of the apposition is maintained at neutral pH, while myelin swells at lower pH (unpublished results). The swelling and compaction at this apposition can be accounted for by a balance between the electrostatic repulsion and van der Waal's attractive forces between membrane surfaces according to DLVO theory of colloid stability [32,33]. An anomalous compaction from the swollen to the native period at neutral pH is interpreted as arising from a conformational change of xP0 due to the interaction between deprotonated His52 and positively charged Arg45′ at this pH [13,32,33]. However, our previous studies indicated that changes in pH and ionic strength, which should inevitably disrupt the electrostatic interaction between His52 and Arg45′, did not have noticeable effect on the relative amount of xP0 dimer. This finding suggested that the interaction between these two residues does not play a major role, if any, in the stability of the xP0 dimer.

Unlike the extracellular apposition, the cytoplasmic apposition of *Xenopus* peripheral myelin remains unchanged at different values of pH and ionic strength, but undergoes swelling in the presence of various detergents, including non-denaturing zwitterionic detergent CHAPSO, non-ionic detergent beta-OG, and cationic detergent DTMAB (Luo et al., unpublished data). This phenomenon indicates that the cytoplasmic apposition is stabilized by certain hydrophobic interactions. However, preliminary studies indicated that similar detergent treatments did not change the level of xP0 dimer in SDS-PAGE gels. While our results suggest that hydrophobic interaction does not play a critical role in stabilizing the dimer, we cannot completely eliminate the possibility that some hydrophobic interaction is involved in xP0 dimerization. Due to the limited number of detergents and incubation conditions tested, some possibility exists that this "unknown" hydrophobic interaction remains intact under our experimental conditions. It was also shown that disruption of disulfide bond in xP0 dimer did not have noticeable effect on its stability, nor did denaturation of the protein by heat or urea [15]. Until now, xP0 dimer has proven to be resistant to all the physical and chemical treatments we performed. At the start of the investigation reported herein, it seemed quite logical to propose that some non-disulfide covalent linkage(s) might be involved in stabilizing the dimer. This proposition led us to undertake the study described here, in an attempt to identify cross-linking site(s) uniquely present in the xP0 dimer.

In the current study, mass spectrometry did not reveal any cross-linked peptide fragments from the in-gel digested xP0 dimer, even when multiple proteases were used. To extend the upper mass range for recovery and detection of the digested peptides, continuous elution preparative gel electrophoresis was performed, with the goal of achieving large-scale purification of xP0 dimer for subsequent in-solution digestion followed by MS analysis. Surprisingly, nearly all the dimer dissociated into monomer during the electro-elution process. This reproducible finding was in striking contrast to the marked stability of xP0 dimer under the various treatments conducted previously, and indicated that covalent bonding is unlikely to be responsible for the dimer formation and stability, since the electro-elution conditions used in the protein fractionation process would not be expected to cleave any covalent bonds. Therefore, the failure of xP0 dimer to dissociate under the experimental conditions used in previous studies might be accounted for by the involvement of multiple types of non-covalent interactions in the formation and maintenance of the dimer. It is likely that these interactions were slowly but completely disrupted, during the more than 10-h elution procedure we used. Future experiments should test this possibility by combining different treatments of the dimer; such results will help to define the specific interactions.

### 4.2. Implication of the observed equilibrium between xP0 dimer and monomer

A dynamic transition between xP0 dimer and monomer was observed by SDS-PAGE: when the gel-purified dimer and monomer were reloaded onto slab gels, around half of the dimer dissociated into monomer, while part of the monomer associated to form dimer. This interesting *in vitro* observation suggests the possibility of an equilibrium between P0 dimer and monomer

populations in the PNS compact myelin of *Xenopus*, i.e., a pool of xP0 monomer may maintain an intrinsic balance with the dimer population, and this balance might be very important in maintaining the plasticity as well as stability of the myelin sheath.

### 4.3. Unique N-glycosylation of xP0

The results presented here show the detailed structural characterization of the *N*-linked glycan profile and identification of glycosylation site of xP0 by sensitive MS techniques. Asn92 was identified and confirmed as the single fully occupied *N*-glycosylation site, and Asn-Gly-Thr was verified to be the *N*-glycosylation motif by ESI MS/MS. The result is consistent with the single conserved *N*-glycosylation site on Asn93 of both rat and bovine P0 that is predicted from the respective cDNA sequences [34,35]. Asn93 has also been proposed to be the only glycosylation site in human P0, based on the observation that oligosaccharides account for only ∼8% of total protein weight, in good agreement with the *N*-glycosylation motif prediction from the human P0 sequence [36,37].

Like the *N*-glycans in higher vertebrate P0, those from xP0 display a high degree of heterogeneity. Moreover, we found that the xP0 glycan chains exhibit new structural features: (1) principally high mannose and hybrid types account for the neutral glycans; (2) among a total of 12 glycans, only 5 acidic components were detected (3 were sialylated and 2 were sulfated); (3) no evidence for core fucose was observed for any of the major glycans; and (4) no glucuronic acid (GlcA) was detected, hence no HNK-1 epitope is present. Our results suggest that most glycoforms from xP0 are tri- and tetra-antennary, and likely are hybrid types with different structures at the Man-4 branch. The fine structures of major oligosaccharides were determined by ESI-FT MS/MS (Fig. 4).

The unique glycan structures of xP0 identified here suggest a species-specific variation of the glycosylation profile when compared with those for P0 from other species such as bovine and human. Use of high resolution magic angle spinning $^{1}$H NMR, MALDI-TOF and ESI-MS, showed that bovine P0 glycans have hybrid (∼75%) and biantennary complex-type glycan structures (∼25%) containing a variety of epitopes including an HNK-1 epitope carrying the characteristic sulfated trisaccharide $SO_4$-3GlcAβ1-3Galβ1-4GlcNAc, and 6-*O*-sulfosialyl-Lewis X. All bovine glycans were core-fucosylated with diverse structures at the Man-4 branch [38,39]. *N*-linked oligosaccharides of human P0 have been characterized by serial lectin affinity chromatography (SLAC) analysis on $^{14}$C-labelled glycopeptides [36,40]. More than 15 different types of glycans were fractionated. Based on the specific radioactivity, human P0 was found to contain ∼82% tri- and tetra-antennary glycan with the HNK-1 epitope, ∼11% biantennary, and ∼7% high-mannose and/or hybrid types of oligosaccharides. In addition, these authors reported that all major types of glycans contain an α(1,6)Fuc residue in the core, belong to the hybrid class and have one or three sulfate residues [41].

### 4.4. Varied glycosylation of P0 may reflect differential expression of glycosyltransferases among species

Species-specific sugar moieties in P0 suggest differential expression levels of glycosyltransferases, although these proteins share highly conserved amino acid sequences among a wide range of phylogenetic species. The initial step of *N*-glycosylation involves the transfer of an *N*-glycan precursor ($Glc_3Man_9GlcNAc_2$) from lipid-linked dolichol to the protein's nascent glycosylation sites [42–44]. As a result, the "core *N*-glycan" structure is the same for all proteins. Subsequent trimming of the precursor by alpha-mannosidases in the ER only introduces limited additional diversity. However, the subsequent addition of other sugar moieties by glycosyltransferases in the Golgi complex can vary significantly, and is dependent on peptide folding and accessibility of the glycosylation sites to glycosylation enzymes [43,45,46]. Furthermore, the distinct glycosylation patterns in glycoproteins likely also reflect quantitative or qualitative changes in the expression of glycosyltransferases. The microheterogeneity in the array of glycoprotein oligosaccharides synthesized in the Golgi compartments results from developmental regulation of glycosyltransferases. Therefore, it is likely that the species-specific variability of P0 glycans results from distinctions in their expression patterns of ER and Golgi glycosyltransferases [47,48]. Thus, the unusual glycosylation profile of P0 in *Xenopus* reported in this study might reflect unique expression levels of the corresponding glycosyltransferases.

The absence of the HNK-1 epitope in *Xenopus* P0 glycans is somewhat unexpected, as it is a well-documented carbohydrate epitope shared by both bovine and human P0. This carbohydrate antigen is recognized by the monoclonal anti-HNK-1 antibody, and prominently expressed in the nervous system on a series of cell adhesion glycoproteins such as myelin-association glycoprotein (MAG) and P0, and some glycolipids such as SGGL-1 and SGGL-2 [49]. It is clear that the sulfate group in the epitope is critical for binding of HNK-1 to its antibody, since complete desulfation abolishes the interaction. The biosynthesis of this epitope is regulated by two glucuronyltransferases (GlcAT-P and GlcAT-S) and a sulfotransferase (HNK-1ST) [50]. The absence of the HNK-1 epitope in xP0 suggests that the relevant glucuronyltransferases and sulfotransferase, if present, are expressed at appreciably lower levels in the peripheral nerves from *Xenopus* than in other species. Furthermore, the absence of core-Fucose on the total glycans from xP0 suggests that expression level of the fucosyltranferase(s) might be very low or restricted under the native conditions. Future studies on the glycosyltransferase activities in peripheral nerves of different species would test this idea.

### 4.5. Carbohydrate moieties might contribute to xP0 aggregation behavior

*N*-Glycosylation differs from other common protein modifications, such as phosphorylation and acetylation, because the glycan is considerably larger than other modifications in both mass and volume. The covalent attachment of heterogeneous,

hydrophilic large glycans to polypeptides can dramatically alter the protein conformation, and thus play a crucial role in promoting of proper folding of nascent polypeptides in the ER. At the same time, glycans can prevent abnormal aggregation of the glycoproteins by providing solubility-enhancing polar surface groups. The inhibition of *N*-glycosylation usually results in severe consequences such as protein misfolding, aggregation, degradation, and loss of function [51–53].

Therefore, it is not surprising that the *N*-linked glycans might play a similar role in the proper folding of P0 in the ER, and hence may facilitate the establishment of the non-covalent interactions that lead to protein multimerization. *In vitro* studies of P0 transfected into cultured mammalian cells have shown that the carbohydrate moieties of P0 affect its activity in cell–cell adhesion via P0 homophilic interactions [5–7]. Although it is not known whether glycosylation influences P0 folding *in vivo*, the unique glycosylation profile of xP0, especially the absence of the HNK-1 epitope, could have functional implications. Since it is known that the expression of the HNK-1 epitope is temporally and spatially regulated during the development of the nervous system, and that this epitope itself confers adhesiveness on neural glycoproteins in general [54–56], it seems possible that the remarkably different glycan structures of xP0 may influence the protein folding and, consequently, result in causing its aggregation behavior to be different P0 from those of the higher vertebrates such as bovine and murine. Site-directed mutagenesis and domain swapping studies could illuminate our understanding of how glycosylation affects the peptide folding and, ultimately, leads to the dimerization of *Xenopus* P0.

Although *N*-linked glycans usually play a critical role during glycoprotein folding, these glycans can be insignificant in maintaining the native structures of mature glycoproteins [51,52,57]. Therefore, the removal of oligosaccharide chains from the mature xP0 might have little effect on the protein's native structure and oligomerization behavior. This is also consistent with the observation that deglycosylation treatment with PNGase F did not change the level of xP0 dimer (Supplementary Fig. 6).

### 4.6. Distinct acylation profile of xP0

We determined that xP0 has a covalently bound long-chain stearoyl group (C18:0), and the acylation site is assigned to Cys152, which is the only potential acylation site in the acylated tryptic peptide (amino acid segment 151–155, Tyr-Cys-Trp-Leu-Arg in Fig. 6). This is consistent with the deduced sequence for xP0 (Luo et al., unpublished) (Supplementary Fig. 2). There are only three cysteine residues in xP0: Cys21, Cys97 in the extracellular domain, and Cys152 in the cytoplasmic domain. The two extracellular Cys residues form an intra-molecular disulfide bond in the Ig fold domain [31]. The availability of the Cys97 site for disulfide bond formation is confirmed by our MS analysis (Fig. 5), since the peptide containing reduced and iodoacetamide-blocked Cys97 was observed and the amino acid sequence was confirmed by ESI-MS/MS (Fig. 5).

Over the last decade, the determination of the acylation profile and exact acylation site in P0 has proven to be challenging owing to the instability of protein–fatty acyl group linkages and the poor recovery of hydrophobic acylated peptides. Our identification of Cys152 as the acylation site in xP0 is consistent with the studies on P0 from higher vertebrates, such as bovine or rat. Although the exact acylation site of bovine P0 has not been experimentally determined, studies have indicated that the fatty acid is attached to one of five potential acylation sites within a tryptic peptide from a transmembrane domain, with Cys153 being the most probable acylation candidate [10]. Other investigators showed that Cys153, the single acylation site in murine P0 from sciatic nerve, bears a thioester linkage [11]. However, while we found xP0 to be highly stearoylated, P0 from rat and bovine are predominantly palmitoylated [10,11]. Analysis of the fatty acids released by hydrolysis of the murine P0 indicated that the fatty acid composition is ∼50% palmitic, ∼40% stearic, and ∼10% oleic acids [11].

Protein acylation is increasingly recognized to play an important role in the nervous system; and the addition of long chain fatty acyl groups greatly enhances the hydrophobicity of myelin proteins [58]. In P0 specifically, the acylated Cys residue is located at the junction of the putative transmembrane and cytoplasmic domains, and the presence of an ∼20-Å long acyl group such as palmitic acid at this specific location may stabilize, via trans interaction, a hydrophobic pocket in the middle of the cytoplasmic apposition [14]. Moreover, even though acylation of membrane protein via thioester linkage occurs as a post-translational modification in protein maturation, this specific modification may take place at an early step in the protein processing, even before the maturation of the glycan structure [59]. Therefore, similar to consequences of variation in *N*-glycosylation, the diverse acylation profiles of P0 from different species may also contribute to the species-specific conformational change of P0, before this protein is incorporated into the myelin membranes. Also, like glycosylation, acylation may help to fold xP0 properly, and thereby to establish non-covalent interactions that underlying to xP0 dimerization. Once these interactions are established, the fatty acyl chain may no longer be required to stabilize the dimer. This scenario is consistent with our observation that the treatment of *Xenopus* peripheral myelin with the deacylation reagent hydroxylamine had no effect on the level of xP0 dimer (data not shown). Future experiments using acylation inhibitors or acylation-deficient mutants may help to elucidate the biological functions played by fatty acylation of xP0 protein.

### 4.7. Biological and phylogenetic implications

Based on the data presented here and in previous studies, we conclude that non-covalent interactions are responsible for *Xenopus* P0 dimerization, although the current data do not define the identities of these interactions. Our results suggest that there is likely a monomer–dimer equilibrium of P0 in compact *Xenopus* PNS myelin, implicating a dynamic turnover of P0 molecular contacts *in vivo* that contributes to the plasticity of the myelin sheath. The aggregation behavior of *Xenopus* P0 is remarkably different from that of the higher vertebrates including mouse and cattle, implicating critical phylogenetic

variations in P0's folding and oligomerization patterns that may be accounted for by the species-specific glycosylation and acylation profiles. In conclusion, our molecular level investigation into the unique oligomerization behavior of xP0 should contribute toward understanding the phylogenetic development of P0's adhesion role in the mature PNS myelin.

## Acknowledgements

We thank Yan Wang, Joseph Zaia, and John Cipollo (all of BU), and Deepak Sharma, Brian Tevlin, Robin Avila, and Hideyo Inouye (all of BC) for valuable suggestions and help. This work was supported by NIH-NCRR P41 RR10888 and S10 RR15942 (to CEC), and Institutional Research Fund from Boston College (to DAK).

## Appendix A. Supplementary data

Supplementary data associated with this article can be found, in the online version, at doi:10.1016/j.ijms.2007.08.007.

## References

[1] D.A. Kirschner, L. Wrabetz, M.L. Feltri, The P0 Gene. In: Myelin Biology and Disorders. Elsevier/Academic Press, NY, 2004, p. 523.
[2] J. Eichberg, Neurochem. Res. 27 (2002) 1331.
[3] K.P. Giese, R. Martini, G. Lemke, P. Soriano, M. Schachner, Cell 71 (1992) 565.
[4] L.E. Warner, M.J. Hilz, S.H. Appel, J.M. Killian, E.H. Kolodry, G. Karpati, S. Carpenter, G.V. Watters, C. Wheeler, D. Witt, A. Bodell, E. Nelis, C. Van Broeckhoven, J.R. Lupski, Neuron 17 (1996) 451.
[5] M. Yoshida, D.R. Colman, Neuron 16 (1996) 1115.
[6] T. Yazaki, M. Miura, H. Asou, K. Kitamura, S. Toya, K. Uyemura, FEBS Lett. 307 (1992) 361.
[7] M.T. Filbin, G.I. Tennekoon, J. Cell. Biol. 122 (1993) 451.
[8] T. Yazaki, M. Miura, H. Asou, K. Kitamura, S. Toya, U. Keiichi, FEBS Lett. 310 (1992) 277.
[9] M.F. Schmidt, Biochim. Biophys. Acta 988 (1989) 411.
[10] Y. Sakamoto, K. Kitamura, K. Yoshimura, T. Nishijima, K. Uyemura, Biomed. Res. (1986) 261.
[11] O.A. Bizzozero, K. Fridal, A. Pastuszyn, J. Neurochem. 62 (1994) 1163.
[12] L.Y. Bourguignon, E.L. Kalomiris, V.B. Lokeshwar, J. Biol. Chem. 266 (1991) 11761.
[13] L. Shapiro, J.P. Doyle, P. Hensley, D.R. Colman, W.A. Hendrickson, Neuron 17 (1996) 435.
[14] H. Inouye, H. Tsuruta, J. Sedzik, K. Uyemura, D.A. Kirschner, Biophys. J. 76 (1999) 423.
[15] A.J. Thompson, M.S. Cronin, D.A. Kirschner, J. Neurosci. Res. 67 (2002) 766.
[16] G. Jeserich, T.V. Waehneldt, Neurochem. Res. 12 (1987) 825.
[17] J. Karthigasan, T.K. Bauer, D.B. Teplow, R.A. Saavedra, D.A. Kirschner, J. Mol. Neurosci. 3 (1992) 185.
[18] W.T. Norton, S.E. Poduslo, J. Neurochem. 21 (1973) 759.
[19] W.T. Norton, S.E. Poduslo, J. Neurochem. 21 (1973) 749.
[20] N.H. Packer, M.A. Lawson, D.R. Jardine, J.W. Redmond, Glycoconj. J. 15 (1998) 737.
[21] S.F. Wheeler, D.J. Harvey, Anal. Biochem. 296 (2001) 92.
[22] I. Ciucanu, F. Kerek, Carbohydr. Res. 131 (1984) 209.
[23] I. Ciucanu, C.E. Costello, J. Am. Chem. Soc. 125 (2003) 16213.
[24] J.A. Jebanathirajah, J.L. Pittman, B.A. Thomson, B.A. Budnik, P. Kaur, M. Rape, M. Kirschner, C.E. Costello, P.B. O'Connor, J. Am. Mass Spectrom. 16 (2005) 1985.
[25] P.B. O'Connor, J.L. Pittman, B.A. Thomson, B.A. Budnik, J.C. Cournoyer, J. Jebanathirajah, C. Lin, S. Moyer, C. Zhao, Rapid Commun. Mass Spectrom. 20 (2006) 259.
[26] P. Chen, A.G. Baker, M.V. Novotny, Anal. Biochem. 244 (1997) 144.
[27] S.F. Wheeler, D.J. Harvey, Anal. Chem. 72 (2000) 5027.
[28] B. Kuster, S.F. Wheeler, A.P. Hunter, R.A. Dwek, D.J. Harvey, Anal. Biochem. 250 (1997) 82.
[29] A.K. Powell, D.J. Harvey, Rapid Commun. Mass Spectrom. 10 (1996) 1027.
[30] B. Domon, C.E. Costello, Glycoconj. J. (1988) 397.
[31] C.A. Wells, R.A. Saavedra, H. Inouye, D.A. Kirschner, J. Neurochem. 61 (1993) 1987.
[32] H. Inouye, D.A. Kirschner, Biophys. J. 53 (1988) 235.
[33] H. Inouye, D.A. Kirschner, Biophys. J. 53 (1988) 247.
[34] Y. Sakamoto, K. Kitamura, K. Yoshimura, T. Nishijima, K. Uyemura, J. Biol. Chem. 262 (1987) 4208.
[35] G. Lemke, R. Axel, Cell 40 (1985) 501.
[36] D. Burger, M. Simon, G. Perruisseau, A.J. Steck, J. Neurochem. 54 (1990) 1569.
[37] K. Hayasaka, K. Nanao, M. Tahara, W. Sato, G. Takada, M. Miura, K. Uyemura, Biochem. Biophys. Res. Commun. 180 (1991) 515.
[38] R.G. Gallego, J.L. Blanco, C.W. Thijssen-van Zuylen, C.H. Gotfredsen, H. Voshol, J.O. Duus, M. Schachner, J.F. Vliegenthart, J. Biol. Chem. 276 (2001) 30834.
[39] H. Voshol, C.W. van Zuylen, G. Orberger, J.F. Vliegenthart, M. Schachner, J. Biol. Chem. 271 (1996) 22957.
[40] D. Burger, G. Perruisseau, M. Simon, A.J. Steck, J. Neurochem. 58 (1992) 845.
[41] M.C. Field, D.R. Wing, R.A. Dwek, T.W. Rademacher, B. Schmitz, E. Bollensen, M. Schachner, J. Neurochem. 58 (1992) 993.
[42] R. Kornfeld, S. Kornfeld, Annu. Rev. Biochem. 54 (1985) 631.
[43] N. Jenkins, R.B. Parekh, D.C. James, Nat. Biotechnol. 14 (1996) 975.
[44] P. Burda, M. Aebi, Biochim. Biophys. Acta 1426 (1999) 239.
[45] J. Jones, S.S. Krag, M.J. Betenbaugh, Biochim. Biophys. Acta (2005).
[46] M.D. Snider, P.W. Robbins, Methods Cell Biol. 23 (1981) 89.
[47] H. Schachter, Biochem. Cell Biol. 64 (1986) 163.
[48] J.C. Paulson, K.J. Colley, J. Biol. Chem. 264 (1989) 17615.
[49] M. Schachner, R. Martini, H. Hall, G. Orberger, Prog. Brain Res. 105 (1995) 183.
[50] S. Oka, K. Terayama, C. Kawashima, T. Kawasaki, J. Biol. Chem. 267 (1992) 22711.
[51] J.C. Paulson, Trends Biochem. Sci. 14 (1989) 272.
[52] A. Helenius, Mol. Biol. Cell 5 (1994) 253.
[53] A. Helenius, M. Aebi, Science 291 (2001) 2364.
[54] G.A. Schwarting, F.B. Jungalwala, D.K. Chou, A.M. Boyer, M. Yamamoto, Dev. Biol. 120 (1987) 65.
[55] Y. Yoshihara, S. Oka, Y. Watanabe, K. Mori, J. Cell. Biol. 115 (1991) 731.
[56] D.K. Chou, A.A. Ilyas, J.E. Evans, C. Costello, R.H. Quarles, F.B. Jungalwala, J. Biol. Chem. 261 (1986) 11717.
[57] K. Olden, J.B. Parent, S.L. White, Biochim. Biophys. Acta 650 (1982) 209.
[58] O.A. Bizzozero, S.U. Tetzloff, M. Bharadwaj, Neurochem. Res. 19 (1994) 923.
[59] A.M. Schultz, L.E. Henderson, S. Oroszlan, Annu. Rev. Cell Biol. 4 (1988) 611.
[60] J. Lemoine, G. Strecker, Y. Leroy, B. Fournet, G. Ricart, Carbohydr. Res. 221 (1991) 209.